

NLO QCD + EW corrections to WWW production with leptonic decays at the LHC

Shen Yong-Bai^a, Zhang Ren-You^a, Ma Wen-Gan^a, Li Xiao-Zhou^a, and Guo Lei^b

^a *Department of Modern Physics, University of Science and Technology of China, Hefei, Anhui 230026, P.R. China*

^b *Department of Physics, Chongqing University, Chongqing 401331, P.R. China*
E-mail: ybshen@mail.ustc.edu.cn, zhangry@ustc.edu.cn, mawg@ustc.edu.cn, lixz0818@mail.ustc.edu.cn, guoleicqu@cqu.edu.cn

ABSTRACT: In this paper we calculate the next-to-leading order (NLO) QCD and NLO electroweak (EW) corrections to WWW production with subsequent W -boson leptonic decays at the LHC by adopting an improved narrow width approximation which takes into account the spin correlation and finite width effects from the W^\pm -boson decays. The NLO QCD correction from gluon-quark reaction channels is discussed, which enhances significantly the NLO QCD correction in high energy region for the transverse momentum and invariant mass distributions of final particle. We provide also the integrated cross section for the WWW production and various kinematic distributions of final products with NLO QCD+EW accuracy. We find by applying a hard jet veto in events selection, we can keep the convergence of the perturbative QCD description and improve the scale uncertainty. Our numerical results show that both the NLO QCD and NLO EW corrections should be considered in precision predictions. We see also that the genuine NLO QCD relative correction to the integrated cross section for $W^+W^-W^+$ production at the 14 TeV LHC, is 28.19% in the jet veto condition of $p_T^{jet} > p_T^{jet,lower} = 50$ GeV, while the pure NLO EW relative corrections can reach 15.15% in inclusive event selection scheme.

KEYWORDS: NLO QCD + NLO EW Corrections, Gauge Couplings, Hadron Colliders .

Contents

1. Introduction	1
2. Calculations	2
2.1 General setup	2
2.2 LO contributions	3
2.3 Virtual corrections	5
2.4 Real corrections	6
3. Numerical results and discussion	7
3.1 Input parameters	7
3.2 Integrated cross sections	8
3.3 Kinematic distributions	10
4. Summary	13

1. Introduction

With the discovery of the Higgs boson by the CERN ATLAS and CMS collaborations [1,2], one of the further goals of the large hadron collider (LHC) is to test the standard model (SM). Precision test of the SM at the LHC requires accurate and reliable phenomenological predictions. Since measuring the gauge couplings is one of the experiments to test SM, we have to make sure that all the couplings predicted by the SM is precisely consistent with experimental measurement in order to confirm the validity of the SM. The gauge couplings are usually tested by vector boson production processes and most of these processes at the LHC have been computed up to QCD next-to-leading order (NLO) so far. The measurements at 14 TeV will be possible in LHC Run 2 with higher luminosity, and the sensitivity to electroweak couplings increases with the reach in the high-energy tails of distributions. Only the NLO QCD prediction alone may not deliver a reliable estimate as expected. Theoretical precision predictions is therefore ahead of us to have a thorough interpretation of data, which can be realized by taking into account electroweak information. It is desired for the calculation of vector boson production in to NLO QCD + NLO EW.

The triple vector boson production processes are sensitive to the triple and quartic gauge couplings (TGCs and QGCs) and thus related to the electroweak symmetry spontaneous breaking (EWSB) mechanism [3,4]. The measurements of the triple gauge boson productions at hadron colliders can provide rich information on the gauge boson self-interactions and play an important role in finding new physics beyond the standard model

(BSM). In order to improve the precision of the theoretical predictions, it is necessary to calculate the $VV'V''$ ($V, V', V'' = W, Z$ or γ) productions at hadron colliders up to NLO QCD + EW including subsequent vector boson decays. The calculation of higher-order terms in the QCD and EW perturbation series for the triple gauge boson productions thus becomes an even more important issue. One can find the requests of this kind of work are listed in the Les Houches 2013 Working Group wishlist [5]. In previous works, all the triple gauge boson productions at hadron colliders, $pp \rightarrow WWZ, ZZZ, WWW, WZZ, WW\gamma, ZZ\gamma, Z\gamma\gamma, \gamma\gamma\gamma, W\gamma\gamma$ and $WZ\gamma$, have been studied in the SM up to the QCD NLO [6–14], while only the $pp \rightarrow WWZ$ and WZZ processes have been complemented by the NLO EW corrections [15, 16], and for the later process the subsequential W - and Z -boson leptonic decays are included.

In this work, we present the NLO QCD + EW corrected integrated cross sections and some kinematic distributions to the $pp \rightarrow WWW + X$ production at the LHC, including the subsequent W -boson leptonic decays. The observables in the WWW production are sensitive to both the triple and the quartic vector boson couplings and thus relevant to study of these anomalous gauge couplings [17, 18]. The NLO QCD correction to WWW production at the LHC was performed before in Refs. [8] [9]. We hereby extend the calculation for WWW production up to QCD + EW NLO including subsequent W -boson leptonic decays to provide more accurate predictions. This paper is organized as follows: In Section 2 we provide the strategy of our calculation. The integrated cross section and various kinematic distributions are presented in Section 3. A summary is given in Section 4.

2. Calculations

2.1 General setup

In the LO and NLO QCD+EW calculations, we adopt the 't Hooft-Feynman gauge, and take into account the Cabibbo-Kobayashi-Maskawa (CKM) mixing between the first two quark generations in all partonic cross sections, but neglect the mixing to the third generation, since it is negligible, i.e., the CKM matrix is $2 \oplus 1$ block-diagonal,

$$V_{CKM} = \left(V_{ij} \right)_{3 \times 3} = \begin{pmatrix} \cos \theta_C & \sin \theta_C & 0 \\ -\sin \theta_C & \cos \theta_C & 0 \\ 0 & 0 & 1 \end{pmatrix}. \quad (2.1)$$

We set the masses of the first two generations of quarks to zero, and adopt the four-flavor scheme in initial-state parton convolution. Therefore, there is no contribution from bottom quark in the initial state and the CKM matrix drops out in the flavour sum of closed fermion loops. The CKM matrix factorizes from all the amplitudes for the WWW production subprocesses, only one generic amplitude has to be evaluated when convoluting the squared matrix elements with the PDFs [16, 19]. Analogously, that is also appropriate for the calculations of the $WWW + g$, $WWW + \gamma$ and $WWW + q$ productions.

We define the NLO QCD and EW relative corrections from $q_1\bar{q}_2 \rightarrow WWW$ and $q_1\gamma \rightarrow WWW + q_2$ partonic processes separately as

$$\delta_{QCD} = \frac{\sigma_{QCD} - \sigma_{LO}}{\sigma_{LO}}, \quad \delta_{EW}^{q\bar{q}} = \frac{\Delta\sigma_{EW}^{q\bar{q}}}{\sigma_0}, \quad \delta_{EW}^{q\gamma} = \frac{\Delta\sigma_{EW}^{q\gamma}}{\sigma_0}, \quad (2.2)$$

where σ_{QCD} , $\Delta\sigma_{EW}^{q\bar{q}}$ and $\Delta\sigma_{EW}^{q\gamma}$ are evaluated with NLO parton distribution functions (PDFs), and σ_{LO} and σ_0 are LO cross sections calculated with LO and NLO PDFs, respectively. Note that unlike the QCD corrections from the quark-antiquark and the gluon-quark induced channels, the EW corrections from the quark-antiquark and the photon-quark induced subprocesses, $\Delta\sigma_{EW}^{q\bar{q}}$ and $\Delta\sigma_{EW}^{q\gamma}$, can be distinguished by their final state products. The numerator $\sigma_{QCD} - \sigma_{LO}$ represents the full NLO QCD correction that includes all the NLO QCD contributions from both the dynamic matrix element and PDFs. To cancel the QCD contribution from NLO PDFs to the NLO EW corrections $\Delta\sigma_{EW}^{q\bar{q}}$ and $\Delta\sigma_{EW}^{q\gamma}$, we normalize the NLO EW relative corrections to σ_0 . In this normalization, the NLO EW relative corrections $\delta_{EW}^{q\bar{q}}$ and $\delta_{EW}^{q\gamma}$ are practically independent of the PDF set.

The pure NLO QCD corrected cross section σ_{QCD} can be expressed as

$$\sigma_{QCD} = \sigma_{LO} (1 + \delta_{QCD}). \quad (2.3)$$

In order to identify potentially large effects due to the interplay between the EW and QCD corrections beyond NLO, we calculate the combined NLO QCD+EW correction by using the naive product in this paper [20],

$$\begin{aligned} \sigma_{NLO} &= \sigma_{LO} (1 + \delta_{NLO}) \\ &= \sigma_{LO} (1 + \delta_{QCD}) (1 + \delta_{EW}^{q\bar{q}} + \delta_{EW}^{q\gamma}), \end{aligned} \quad (2.4)$$

where σ_{NLO} is the NLO QCD+EW corrected cross section and δ_{NLO} is the NLO QCD+EW relative correction. This definition is typically used in observables that receive extremely large QCD corrections.

2.2 LO contributions

The LO contributions to the $W^+W^-W^+$ and $W^+W^-W^-$ productions at the LHC come from the following partonic processes:

$$\begin{aligned} q_1(p_1) + \bar{q}_2(p_2) &\rightarrow W^+(p_3) + W^-(p_4) + W^+(p_5), \\ \bar{q}_1(p_1) + q_2(p_2) &\rightarrow W^+(p_3) + W^-(p_4) + W^-(p_5), \quad (q_1 = u, c, q_2 = d, s), \end{aligned} \quad (2.5)$$

respectively. The parton-level cross section for the $\bar{q}_1q_2 \rightarrow W^+W^-W^-$ process in the SM should be the same as for the $q_1\bar{q}_2 \rightarrow W^+W^-W^+$ process due to the CP conservation. Therefore, we describe the LO and NLO calculations only for the first subprocess in (2.5) in the following.

The LO Feynman diagrams for the partonic process $q_1\bar{q}_2 \rightarrow W^+W^-W^+$ are shown in Fig.1. There are 17 diagrams for each initial quark pair at LO. Fig.1(a) associates with

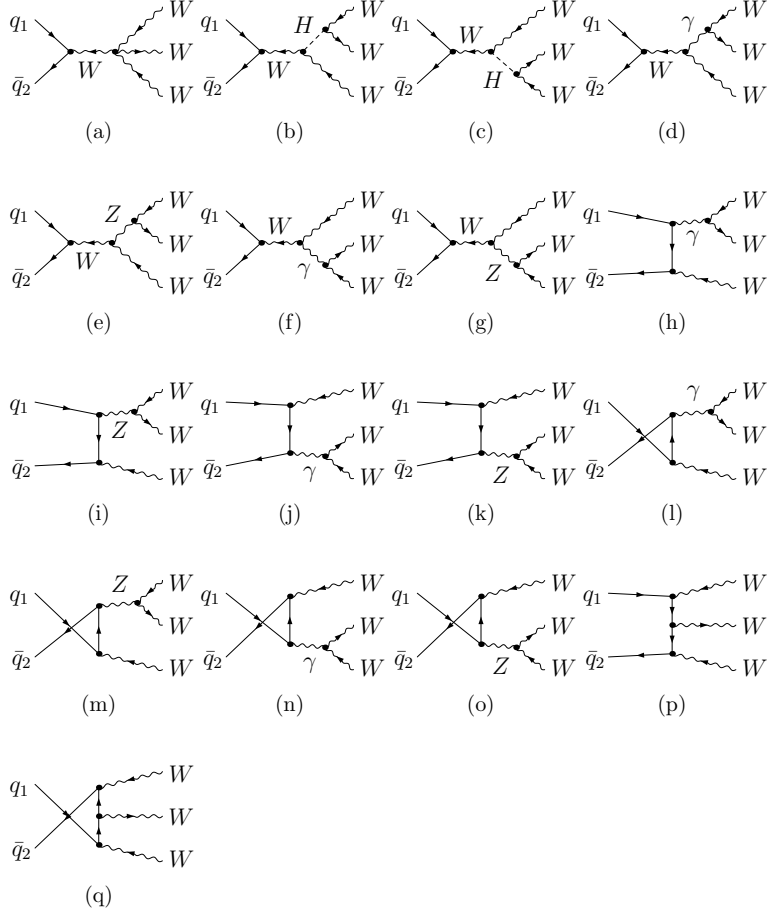


Figure 1: The LO Feynman diagrams for the $q_1 \bar{q}_2 \rightarrow W^+ W^- W^+$ partonic process, where H represents the Higgs boson.

QGC and diagrams (d-o) are related to TGCs. The LO cross section for this partonic process is expressed as

$$\sigma_{LO}^{q_1 \bar{q}_2}(\hat{s}) = \frac{1}{2} \frac{1}{2\hat{s}} \int \overline{\sum} |\mathcal{M}_{LO}^{q_1 \bar{q}_2}|^2 d\Omega_3, \quad (2.6)$$

where the factor $\frac{1}{2}$ arises from the two identical particles in the final state. The summation \sum is taken over the spins of the final state, and the bar over the summation represents averaging over the spins and colors of the initial state. $\mathcal{M}_{LO}^{q_1 \bar{q}_2}$ is the LO amplitude for the $q_1 \bar{q}_2 \rightarrow W^+ W^- W^+$ partonic process, and $d\Omega_3$ is the three-body final state phase space element defined as

$$d\Omega_3 = (2\pi)^4 \delta^{(4)}(p_1 + p_2 - p_3 - p_4 - p_5) \frac{d^3 \vec{p}_3}{(2\pi)^3 2E_3} \frac{d^3 \vec{p}_4}{(2\pi)^3 2E_4} \frac{d^3 \vec{p}_5}{(2\pi)^3 2E_5}. \quad (2.7)$$

The final produced W^\pm -bosons are unstable particles, and we consider their leptonic decays in investigating the final products. In order to take into account the off-shell contribution and spin correlation from the W^\pm -boson leptonic decays, we transform the differential cross sections into Les Houches event files [21, 22] and use MADSPIN to obtain events

after the vector boson decays. Since the spin correlation affects some lepton distributions significantly, Refs. [23, 24] introduced the MADSPIN method which includes the spin correlation. The MADSPIN program is part of MADGRAPH5_AMC@NLO package [25], which can be used to generate the heavy resonance decay preserving both spin correlation and finite width effects to a very good accuracy.

2.3 Virtual corrections

The calculations of the virtual QCD and EW corrections to the partonic process $q_1 \bar{q}_2 \rightarrow W^+ W^- W^+$ are described as below. The IR/UV safety of physical observables requires the cancellation of singularities to all orders. In our discussion, the singularities are isolated by using the dimension regularization (DR) scheme in $D = 4 - 2\epsilon$ dimensions. We adopt the on-mass-shell scheme to renormalize the masses and wave functions for QCD/EW corrections. The UV divergences in QCD/EW one-loop virtual corrections are removed after renormalization. We take the definitions for the relevant EW renormalization constants being same as in Ref. [26]. The expressions for the relevant renormalization constants and the unrenormalized EW self-energies can be found in [26].

We now discuss the issue of EW renormalization for the electric coupling constant. The bare electric charge is related to the renormalized electric charge by definition of $e_0 = (1 + \delta Z_e)e$. By means of the on-shell condition for the coupling of $e-e-\gamma$ three-point function in the Thomson limit and the Ward identity, the electric charge renormalization constant δZ_e in the $\alpha(0)$ -scheme can be written as [26]

$$\delta Z_e^{\alpha(0)} = -\frac{1}{2}\delta Z_{AA} - \frac{1}{2}\tan\theta_W\delta Z_{ZA} = \frac{1}{2}\frac{\partial \sum_T^{AA}(p^2)}{\partial p^2}\Big|_{p^2=0} - \tan\theta_W\frac{\sum_T^{AZ}(0)}{M_Z^2}, \quad (2.8)$$

where θ_W is the weak mixing angle, and $\sum_T^{ab}(p^2)$ denotes the transverse part of the unrenormalized self-energy at four-momentum squared p^2 . However, in the soft limit $p^2 \rightarrow 0$, the photon self-energy induces large logarithmic terms of $\log(m_f^2/\mu^2)$ where m_f is the light fermion mass and μ is the typical scale of a process. In the $\alpha(0)$ -scheme, each external photon leads to a wave-function renormalization constant $\frac{1}{2}\delta Z_{AA}$, which exactly cancels the large logarithms appearing in the corresponding electric charge renormalization constant δZ_e . The logarithms remains for a LO process whose number of external photons is less than the number of EW couplings, the universal uncanceled large logarithms have to be absorbed into the running of α using the $\alpha(M_Z^2)$ - or G_μ -scheme. In this work we take the G_μ -scheme with

$$\alpha_{G_\mu} = \frac{\sqrt{2}G_\mu M_W^2}{\pi} \left(1 - \frac{M_W^2}{M_Z^2}\right), \quad (2.9)$$

where G_μ is the Fermi constant. And the electric charge renormalization constant in the G_μ -scheme should be expressed as

$$\delta Z_e^{G_\mu} = \delta Z_e^{\alpha(0)} - \frac{1}{2}\Delta r, \quad (2.10)$$

where Δr corresponds to the subtraction of the logarithmic divergence contributed by the light quarks to δZ_{AA} which was absorbed by α_{G_μ} [26, 27]. For the subprocesses with one external photon leg, i.e., the real photon emission photon-induced partonic processes, the additional electromagnetic coupling was retained in $\alpha(0)$ -scheme. Then we have $\sigma_{LO} \propto \alpha_{G_\mu}^3$ and $\Delta\sigma_{EW} \propto \alpha(0)\alpha_{G_\mu}^3$.

After renormalizing the relevant constants, the QCD/EW one-loop virtual correction to the $q_1\bar{q}_2 \rightarrow W^+W^-W^+$ partonic process is UV-finite but still contains soft and collinear IR singularities. The cancellation of IR singularities in loops requires bremsstrahlung processes which involve an additional gluon/photon. The soft IR singularity is canceled exactly by that in the real gluon/photon emission processes, while the collinear IR singularity is only partially canceled and the remaining collinear IR singularity is absorbed by the collinear gluon/photon emission parts of the related quark PDF QCD/EW counterterms. The representations for quark PDF QCD and EW counterterms, $\delta\Phi_{q|P}^{QCD}$ and $\delta\Phi_{q|P}^{EW}$, are provided in Ref. [16].

We employ the modified FEYNARTS-3.7 package [28] to generate Feynman diagrams and their corresponding amplitudes. The reduction of output amplitudes are implemented by the FORMCALC-7.3 package [29]. The one-loop amplitude can be represented in terms of standard matrix elements. All 5-point integrals are directly reduced to 4-point integrals [30]. The N -point tensor integrals with $N \leq 4$ are computed by means of the Passarino-Veltman reduction formalism [31]. In the calculation of 4-point tensor integrals with rank $n > 3$, the numerical result becomes unstable due to the Gram matrix with small determinant in the reduction equations. In order to deal with numerical instability as well as save CPU time, we developed our codes based on the LOOPTOOLS-2.8 [29, 32] package to calculate the scalar and tensor integrals, which can automatically switch to the quadruple precision arithmetic in case it has to be applied.

2.4 Real corrections

The real correction to the parent process $pp \rightarrow W^+W^-W^+ + X$ includes the real gluon/photon emission corrections and quark-gluon/photon-induced corrections. Since the cancellation of collinear singularities between real gluon/photon emission and virtual corrections is only partial in general, the quark PDF counterterms are introduced to absorb the remaining singularity. The quark-gluon/photon-induced corrections only contain collinear IR singularities, and can be canceled exactly by the collinear quark emission parts of the PDF counterterms.

In our NLO calculation we adopt the two cutoff phase space slicing (TCPSS) technique to isolate the IR singularities for the real emission partonic processes [33]. Two cutoffs δ_s and δ_c are introduced to separate the phase space of the real gluon emission process $q_1(p_1) + \bar{q}_2(p_2) \rightarrow W^+(p_3) + W^-(p_4) + W^+(p_5) + g/\gamma(p_6)$ into soft region ($E_6 \leq \delta_s\sqrt{\hat{s}}/2$), hard collinear region ($E_6 > \delta_s\sqrt{\hat{s}}/2$ and $\min\{\hat{s}_{16}, \hat{s}_{26}\} \leq \delta_c\hat{s}$) and hard noncollinear region ($E_6 > \delta_s\sqrt{\hat{s}}/2$ and $\min\{\hat{s}_{16}, \hat{s}_{26}\} > \delta_c\hat{s}$). The quark-gluon/photon-induced emission processes contain only collinear IR singularities, therefore we only separate their phase space into collinear ($\hat{s}_{26} \leq \delta_c\hat{s}$) and noncollinear ($\hat{s}_{26} > \delta_c\hat{s}$) regions. The cross sections over the soft and (hard) collinear regions contain only the soft and collinear IR singularities separately,

while the cross sections over the (hard) noncollinear regions are IR-finite. We have checked numerically the cutoff independence of the total cross sections for these subprocesses by setting $\delta_c = \delta_s/50$ and varying δ_s from 10^{-5} to 10^{-3} .

In Ref. [8] the authors took the same input parameters as in Ref. [9] and made a numerical comparison for the $pp \rightarrow W^+W^-W^+ + X$ process at the $\sqrt{S} = 14$ TeV LHC. We follow their input parameters and settings, and present a comparison between our numerical results for the LO and NLO QCD corrected integrated cross sections and the corresponding ones provided in Ref. [8] and Ref. [9] in Table 1. It shows that all these numerical results are in good agreement with each other within the Monte Carlo errors.

scale	program	$\sigma_{LO} [fb]$	$\sigma_{QCD} [fb]$
$3m_Z/2$	ours	82.62(3)	152.44(9)
	Ref. [9]	82.7(1)	152.5(3)
	Ref. [8]	82.7(5)	153.2(6)
$3m_W$	ours	82.74(3)	145.17(6)
	Ref. [9]	82.8(1)	145.2(3)
	Ref. [8]	82.5(5)	146.2(6)
$6m_Z$	ours	82.47(3)	136.89(8)
	Ref. [9]	82.4(1)	136.8(3)
	Ref. [8]	81.8(5)	139.1(6)

Table 1: Comparison of our numerical results for the LO and NLO QCD corrected integrated cross sections with the corresponding ones in previous works [8,9]. All input parameters and settings are taken from Ref. [8].

In the discussion for the NLO EW correction to the $pp \rightarrow W^+W^-W^+ \rightarrow \ell_1^+ \nu_{\ell_1} \ell_2^- \nu_{\ell_2} \ell_3^+ \nu_{\ell_3} + X$ process, we neglect the contribution from the real photon radiation off the final charged leptons. The emission of photons collinear with charged lepton ℓ with small mass leads to large logarithms of the form $\alpha^n \ln^n(m_\ell^2/\mu^2)$, where μ denotes a characteristic scale of the process. For final-state radiation (FSR), the logarithms are universal and only influence the kinematics and acceptance of the outgoing particles. The Kinoshita-Lee-Nauenberg (KLN) theorem [34, 35] guarantees that these logarithms cancel if collinear lepton-photon systems are treated fully inclusively. For differential observables the FSR corrections can be reduced by a procedure known as photon recombination, which treats collinear lepton-photon systems as one quasi-particle, named as a dressed lepton [36]. In our calculation the charged leptons are treated as dressed leptons, thus the cross section does not depend on the masses of the leptons and is free of the FSR corrections.

3. Numerical results and discussion

3.1 Input parameters

The following SM input parameters from Ref. [37] are adopted:

$$M_W = 80.385 \text{ GeV}, \quad M_Z = 91.1876 \text{ GeV}, \quad M_t = 173.21 \text{ GeV},$$

$$G_F = 1.16638 \times 10^{-5} \text{ GeV}^{-2}, \quad \alpha(0) = 1/137.036, \quad \alpha_s(m_Z) = 0.119. \quad (3.1)$$

The Higgs-boson mass is fixed as $M_H = 125.09 \text{ GeV}$. All quarks and leptons except top quark are treated as massless and the CKM matrix elements are taken as

$$V_{CKM} = \begin{pmatrix} V_{ud} & V_{us} & V_{ub} \\ V_{cd} & V_{cs} & V_{cb} \\ V_{td} & V_{ts} & V_{tb} \end{pmatrix} = \begin{pmatrix} 0.97425 & 0.22547 & 0 \\ -0.22547 & 0.97425 & 0 \\ 0 & 0 & 1 \end{pmatrix}. \quad (3.2)$$

We set the factorization and renormalization scales being equal and define the central scale as $\mu_0 = \frac{3}{2}M_W$. The two cutoffs are set to be $\delta_s = 10^{-3}$, $\delta_c = 2 \times 10^{-5}$ in NLO QCD calculation, and $\delta_s = 10^{-4}$, $\delta_c = 2 \times 10^{-6}$ in NLO EW calculation separately.

Theoretically, a NLO QCD/EW correction should be also involved in the PDFs when we process the full NLO QCD/EW calculation. However, In the NNPDF PDF set [38] the NNPDF PDF2.3QED only includes QED correction at $\mathcal{O}(\alpha)$. In the calculation of the NLO QCD corrections, we adopt the NLO NNPDF2.3QED PDFs with the \overline{MS} factorization scheme. While for the NLO EW corrections we use the NLO NNPDF2.3QED PDFs with the DIS factorization scheme [39]. The matrix elements are evaluated using the \overline{MS} running strong coupling constant $\alpha_s(\mu)$ with five active flavors provided by the PDF set.

3.2 Integrated cross sections

In Table 2, we present integrated cross section results for the $W^+W^-W^\pm$ productions at the 8 TeV and 14 TeV LHC by taking $\mu_F = \mu_R = \mu_0$. For the QCD corrections to the $W^+W^-W^+$ production, we find that the real light-quark emission correction amounts to 46.0% of the full NLO QCD correction at the 14 TeV LHC, while the virtual and real gluon emission as well as PDF corrections contribute a proportion of 54.0%. In order to keep the convergence of the perturbative QCD description of the $pp \rightarrow W^+W^-W^\pm + X$ processes, we may impose a tight jet veto which can heavily suppress the large QCD correction. We call the event selection scheme with jet veto in condition of $p_T^{jet} > p_{T,lower}^{jet} = 50 \text{ GeV}$ as the exclusive scheme (Scheme (II)) and that without any cut as the inclusive scheme (Scheme (I)). In this table we list the cross sections and relative corrections in both the inclusive and the exclusive event selection schemes at the 8 TeV and 14 TeV LHC. From the table we can see that the photon-induced channels have surprisingly large impact on the NLO EW correction. The NLO EW correction can be heavily suppressed by applying a jet veto event selection scheme. For example, the photon-induced EW relative correction $\delta_{EW}^{q\gamma}$ is 19.46% in the Scheme I, but is reduced to 2.36% after applying a jet veto with condition of $p_T^{jet} > 50 \text{ GeV}$ for the $pp \rightarrow W^+W^-W^+ + X$ process at the 14 TeV LHC. It implies that the theoretical uncertainty from the photon PDF can be reduced by adopting the jet veto event selection scheme. In both two event collection schemes, the quark-antiquark and photon-induced EW corrections have the opposite sign. And the full NLO EW relative correction to the $W^+W^-W^+$ production in the Scheme (I) at the 14 TeV LHC can reach about 15.15%.

Now we discuss the factorization/renormalization scale dependence of the integrated cross sections for $pp \rightarrow W^+W^-W^+ + X$ processes. The factorization scale μ_F affects

process	$\sqrt{S} = 8 \text{ TeV}$		$\sqrt{S} = 14 \text{ TeV}$	
	$pp \rightarrow W^+W^-W^+$	$pp \rightarrow W^+W^-W^-$	$pp \rightarrow W^+W^-W^+$	$pp \rightarrow W^+W^-W^-$
$\sigma_{LO} [fb]$	32.973(6)	15.487(3)	78.65(1)	41.862(9)
$\sigma_{QCD}^{(I)} [fb]$	61.29(2)	30.998(9)	163.20(3)	92.58(4)
$\sigma_{QCD}^{(II)} [fb]$	43.69(2)	22.175(9)	100.82(4)	57.31(4)
$\sigma_{NLO}^{(I)} [fb]$	67.71(4)	35.18(3)	187.92(9)	109.21(7)
$\sigma_{NLO}^{(II)} [fb]$	42.95(3)	22.00(3)	98.85(6)	56.73(5)
$\delta_{QCD}^{(I)} [\%]$	85.88	100.16	107.50	121.16
$\delta_{QCD}^{(II)} [\%]$	32.50	43.18	28.19	36.90
$\delta_{EW}^{(I)} [\%]$	10.47	13.48	15.15	17.96
$\delta_{EW}^{(II)} [\%]$	-1.70	-0.79	-1.95	-1.02
$\delta_{EW}^{qq} [\%]$	-3.68	-3.30	-4.31	-3.85
$\delta_{EW}^{q\gamma(I)} [\%]$	14.15	16.78	19.46	21.81
$\delta_{EW}^{q\gamma(II)} [\%]$	1.98	2.51	2.36	2.83

Table 2: The LO, NLO QCD, NLO EW and NLO QCD+EW corrected integrated cross sections for the $pp \rightarrow W^+W^-W^\pm + X$ process and the corresponding relative corrections at the LHC with $\sqrt{S} = 8$ and 14 TeV by adopting the Scheme (I) and Scheme (II) event selection strategies.

both the LO and the NLO results. Since the triple vector boson production is a purely electroweak process, there is no renormalization scale dependence at LO. In our NLO EW calculation for the $q_1\bar{q}_2 \rightarrow W^+W^-W^+$ subprocess, we take the G_μ -scheme and for the real photon emission subprocess we use $\alpha(0)$ -scheme instead of G_μ -scheme, Then there does not introduce any μ_R dependence. But the renormalization scale μ_R occurs via the strong coupling constant $\alpha_s(\mu_R)$ and strongly affects the QCD corrections. For simplicity we set $\mu_F = \mu_R = \mu$ in our calculation.

μ	$\sigma_{LO} [fb]$	Scheme (I)		Scheme (II)	
		$\sigma_{QCD} [fb]$	$\sigma_{NLO} [fb]$	$\sigma_{QCD} [fb]$	$\sigma_{NLO} [fb]$
$\mu_0/4$	76.00(1)	189.16(3)	214.5(1)	101.89(3)	99.33(6)
$\mu_0/2$	77.63(1)	174.47(3)	198.79(9)	101.17(3)	98.94(6)
μ_0	78.65(1)	163.20(3)	187.05(9)	100.82(4)	98.92(6)
$2\mu_0$	79.20(1)	154.68(3)	178.43(8)	100.94(3)	99.32(6)
$4\mu_0$	79.36(1)	147.98(3)	171.91(7)	101.16(3)	99.85(5)

Table 3: The factorization/renormalization scale dependence of σ_{LO} , σ_{QCD} and σ_{NLO} for the $W^+W^-W^+$ production at the 14 TeV LHC by adopting the Scheme (I) and Scheme (II) event selection strategies.

In Table 3 we show the LO, NLO QCD, NLO EW and NLO QCD+EW corrected total cross sections (σ_{LO} , σ_{QCD} and σ_{NLO}) for the $W^+W^-W^+$ production at the 14 TeV LHC as functions of μ varying from $\mu_0/4$ to $4\mu_0$ by adopting the Scheme (I) and Scheme (II) event selection criteria, respectively. To estimate the theoretical scale uncertainty quantitatively,

we define the scale uncertainty as

$$\eta = \frac{\max \left\{ \sigma(\mu) \mid 0.25\mu_0 \leq \mu \leq 4\mu_0 \right\} - \min \left\{ \sigma(\mu) \mid 0.25\mu_0 \leq \mu \leq 4\mu_0 \right\}}{\sigma(\mu_0)}. \quad (3.3)$$

Then we obtain $\eta = 4.3\%$ for the LO cross section, and for the NLO QCD corrected cross section the scale uncertainties are 25.2% and 1.1% in the inclusive and exclusive event collection schemes respectively. We can see that the scale uncertainty at the LO is much less than at the QCD NLO, that is because the strong coupling α_s is not involved in the LO matrix elements. If we take the NLO EW correction together with the QCD NLO correction into consideration, $\eta = 22.8\%$ and 0.9% for integrated corrected cross sections in the Scheme (I) and Scheme (II), respectively. We can conclude that the scale uncertainty of the NLO QCD+EW corrected cross section mainly comes from the NLO QCD correction.

From the above numerical results, we can have the following four points: (1) The NLO QCD correction is very large and ruins the convergence of the perturbative QCD description in the Scheme I. (2) The NLO QCD correction mainly comes from the real jet radiation subprocesses, since the lowest level real jet emission subprocesses are at $\mathcal{O}(\alpha_s(\mu_R))$ which contribute to NLO QCD correction for the first time. That correction part related to the strong coupling constant varies largely with the running of μ_R . Therefore, the scale uncertainty can be heavily reduced by adopting the exclusive event selection scheme with a jet veto. But a tight jet veto would introduce a new source of theoretical uncertainties from various other processes. (3) Due to the small scale dependence of PDFs in the Feynman- x region, the scale dependence of the LO cross section is not apparent. But the LO scale uncertainty does not give a good estimate of the higher order QCD contribution. (4) Compared to the NLO QCD correction, the NLO EW correction is insensitive to the factorization/renormalization scale.

3.3 Kinematic distributions

In this subsection we take the $W^+W^-W^+$ production as an example for WWW productions, and study quantitatively the LO, NLO QCD and NLO QCD+EW corrected differential cross sections of various observables for the $pp \rightarrow W^+W^-W^+ + X$ process. We also show the EW relative corrections via the $q_1\bar{q}_2$ and $q\gamma$ channels as well as the NLO QCD corrections in event selection criteria Scheme (I) and Scheme (II) for each distribution separately.

In Figs.2(a,b), we provide the invariant mass distributions of the $W^+W^-W^+$ system in both the Scheme (I) and Scheme (II) event selection strategies. The relative corrections are depicted in the nether plots. From Fig.2(a) we can see that the QCD relative correction in the Scheme (I) can reach 153.0% in the vicinity of $M_{WWW} = 1200$ GeV. The NLO QCD relative correction to the M_{WWW} distribution in the Scheme (I) is more dependent on the phase space than in the Scheme (II). This is due to the fact that the NLO QCD correction part from gluon-induced channels $pp \rightarrow qg \rightarrow W^+W^-W^+ + q'$ causes large contribution which is more closely related to the phase space. We see also the large QCD correction comes from the $W^+W^-W^+ + jet$ production, and that process with a hard jet

could be better to be considered as belonging to another production process other than the $W^+W^-W^+$ production process. Then we can keep the convergence of the perturbative QCD description and obtain moderate NLO QCD correction by adopting the exclusive event selection scheme. In other words, we can take a jet veto scheme which discards the event with jet having $p_T^{jet} > 50$ GeV, i.e. the Scheme (II), which makes the NLO QCD correction becomes smaller. Actually, the jet veto scheme suppresses the contribution from the real QCD corrections and especially from the gluon-induced channels. However, a jet veto scheme as tight as the condition of $p_T^{jet} > 50$ GeV introduces a new source of theoretical scale uncertainty, as known from various processes. Such scale uncertainty could be analyzed by delicate jet veto resummations. From Fig.2(b) we find that the $q_1\bar{q}_2$ -induced EW correction gives a large negative contribution in the high invariant mass range owing to the so-called EW Sudakov logarithms [40, 41]. The $q\gamma$ -induced EW correction is positive and becomes larger with the increment of the invariant mass. Same as the $q\bar{q}$ channel, the $q\gamma$ channel with a final hard jet is more appropriate to be treated as a $2 \rightarrow 4$ process. The jet veto scheme decreases the $q\gamma$ relative correction from 90.8% to 9.2% at the position around $M_{WWW} \sim 1200$ GeV, showing that the large correction effects are caused by hard jet emission. We conclude that by adopting the Scheme (II) selection criterion, we can suppress the EW relative correction from $q\gamma$ channel, and then the $q_1\bar{q}_2$ -induced EW relative correction becomes dominant in high invariant mass range.

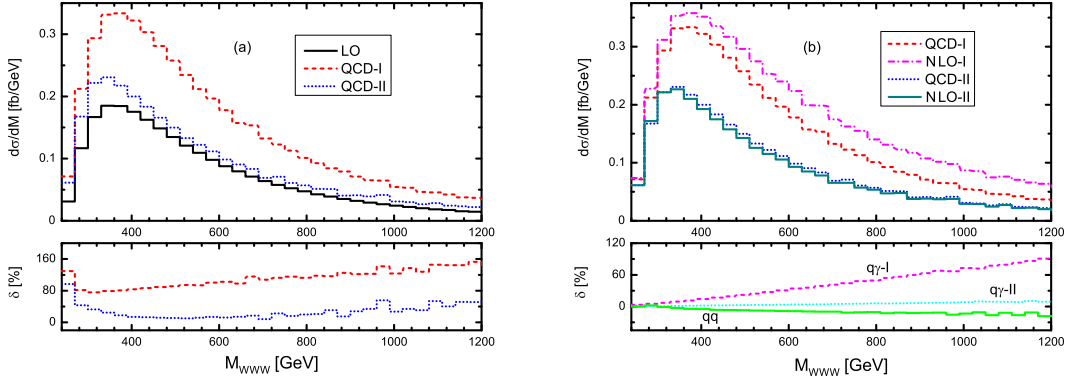


Figure 2: The differential cross sections of $W^+W^-W^+$ invariant mass and the relative corrections for $pp \rightarrow W^+W^-W^+ + X$ process at the 14 TeV LHC in the Scheme (I) and Scheme (II) event selection schemes. (a) The LO and NLO QCD corrected distributions and the corresponding relative corrections. (b) The NLO QCD+EW corrected distributions. The corresponding NLO QCD corrected distributions are also plotted for comparison. In the nether plot, the NLO EW relative corrections from photon-induced channels in two schemes, and the NLO EW relative correction from the $pp \rightarrow q_1q_2 \rightarrow W^+W^-W^+$ channels are depicted separately.

In Figs.3(a,b) we show the LO and NLO corrected rapidity distributions of $W^+W^-W^+$ system by adopting the inclusive and exclusive event selection schemes. Fig.3(a) shows the LO and NLO QCD corrected WWW rapidity distributions. From this figure we can see that the NLO QCD relative corrections at the position of $y_{WWW} = 0$ in the Scheme (I) and Scheme (II) event selection schemes are about 123.7% and 17.4%, respectively. With the

increment of $|y_{WWW}|$, the QCD relative correction in the Scheme (I) decreases, while in the the Scheme (II) it increases smoothly. We see that the NLO QCD relative correction in the Scheme (II) heavily reduces the corresponding one in the Scheme (I), particularly at the position around $|y_{WWW}| \sim 0$. As we know, the events with high WWW system transverse momentum, tend to be produced centrally (i.e., the position of $y_{WWW} \rightarrow 0$), and will be excluded in the Scheme (II) case due to the jet veto. That's why the NLO QCD relative correction in the Scheme (II) is obviously suppressed in the small $|y_{WWW}|$ range. As we can see from Fig.3(b), the EW relative correction to the $pp \rightarrow q_1 q_2 \rightarrow W^+ W^- W^+ + X$ process is negative and almost constant in the whole plotted range. The absolute EW relative rapidity correction to the photon-induced channel in the Scheme (I) is quantitatively larger than that to the $pp \rightarrow q_1 q_2 \rightarrow W^+ W^- W^+ + X$ process. However, the EW relative correction from the photon-induced channel in the Scheme (II) becomes even smaller when the jet veto is applied and is stable in the whole plotted range. We see from Fig.3(b) that the NLO QCD+EW relative correction in the Scheme (II) slightly suppresses the corresponding NLO QCD corrected y_{WWW} distribution.

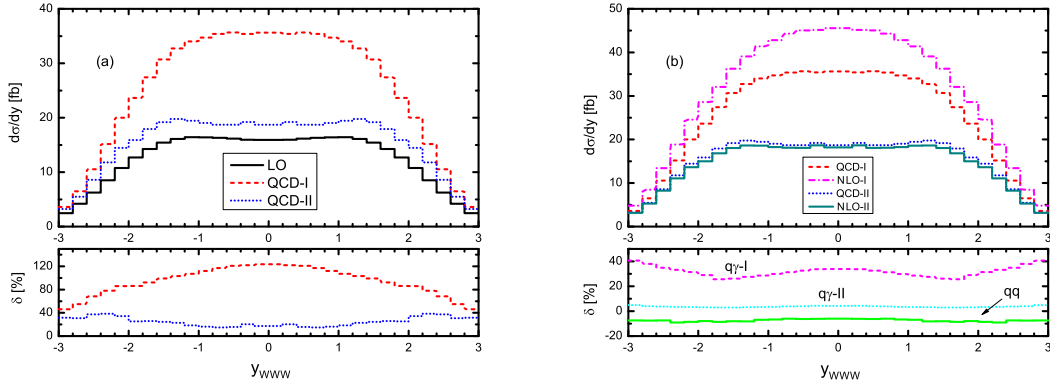


Figure 3: Same as Fig.2 but for the rapidity of the $W^+W^-W^+$ system.

Now we turn to discuss the $W^+W^-W^+ + X$ production with subsequent W -boson leptonic decays ($W \rightarrow \ell \nu_\ell$, $\ell = e, \mu, \tau$). In Figs.4(a,b) and Figs.5(a,b) we display the transverse momentum distributions of the leading lepton and next-to-leading lepton for $pp \rightarrow W^+W^-W^+ \rightarrow \ell_1^+ \nu_{\ell_1} \ell_2^- \nu_{\ell_2} \ell_3^+ \nu_{\ell_3} + X$ in both the inclusive and exclusive event collection schemes. The final lepton with the largest transverse momentum among all leptons is defined as the leading lepton and that with the second largest transverse momentum is called as the next-to-leading lepton. The branch ratios for the W^\pm -boson leptonic decay modes are obtained by using the MADSPIN program. We see from Figs.4(a) that when $p_T^{L-lep} > 50$ GeV, the NLO QCD relative correction in the Scheme (I) goes up with the increment of p_T^{L-lep} . We can read out from Fig.4(a) that the NLO QCD relative correction in the Schemes (I) increases from 40.3% to 393.3% with the increment of p_T^{L-lep} from 50 GeV to 250 GeV. The large NLO QCD correction in high p_T^{L-lep} region and p_T^{L-lep} -dependence of the relative corrections can be traced to the kinematics of the gluon-induced channel contributions [8, 15]. The NLO QCD relative correction can be suppressed by imposing a

jet veto in condition of $p_T^{jet} > 50$ GeV. By contrast, we can read from Fig.4(a) the NLO QCD relative correction in the Scheme (II) ranges from -10.9% to 164.5% with p_T^{L-lep} varying in the same range. While the EW relative corrections to $q_1 q_2$ and $q\gamma$ induced processes decreases and increases with the increment of p_T^{L-lep} , respectively, as shown in the nether plot in Fig.4(b). By adopting the Scheme (II), the relative correction to $q\gamma$ induced process is surprisingly reduced in comparing with that using the Scheme (I). We see also from Figs.5(a,b) that the distribution line-shapes for the transverse momentum of the next-to-leading lepton are alike to the corresponding ones for the leading lepton, and have similar behavior.

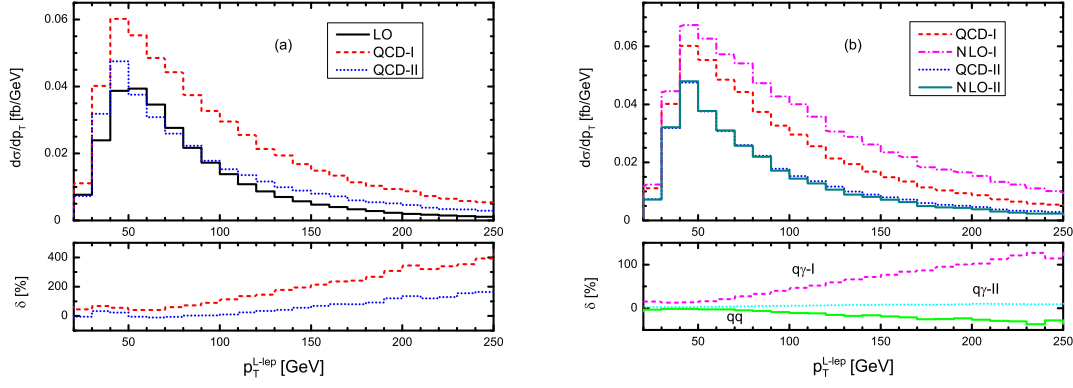


Figure 4: Same as Fig.2 but for the transverse momentum of the leading lepton for the $pp \rightarrow W^+ W^- W^+ \rightarrow \ell_1^+ \nu_{\ell_1} \ell_2^- \nu_{\ell_2} \ell_3^+ \nu_{\ell_3} + X$ process at the 14 TeV LHC.

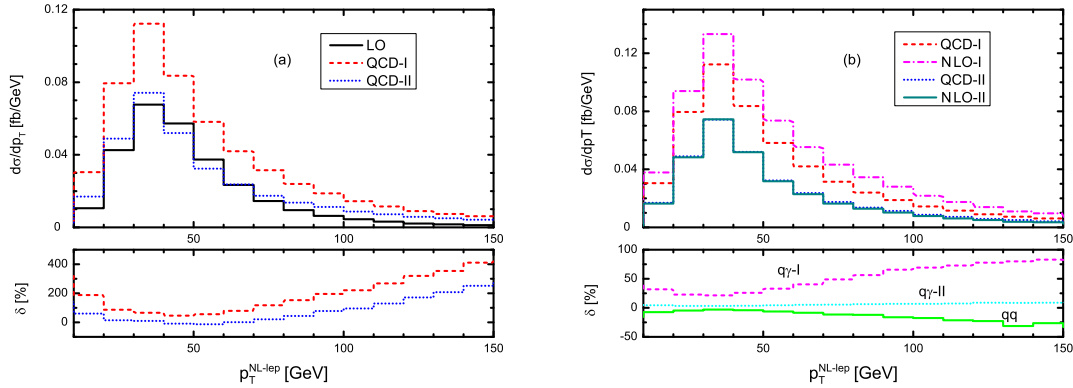


Figure 5: Same as Fig.4 but for the transverse momentum of the next-to-leading lepton.

4. Summary

The triple W -boson production process is an ideal process for determining triple and quartic gauge couplings and understanding EW symmetry breaking as well as the background

to new physics signature. In this work, we calculate the NLO QCD plus NLO EW corrections to the WWW production including subsequent leptonic decays at the LHC. In our calculation we adopt the MADSPIN method which preserves both spin correlation and finite width effect with a very good accuracy. We provide the NLO QCD+EW corrected integrated cross section and some kinematic distributions of final products. We find that the NLO QCD correction part in the inclusive event selection scheme from the gluon-induced production channels with four-particle final particles, enhances heavily the distributions for the final particle transverse momentum and invariant mass, particularly in the high energy regimes, and leads to a comparatively large scale uncertainty. Because in the final state of quark-photon induced channels there also exists a hard jet, its contribution in the inclusive scheme gives a large EW correction impact on p_T and M_{WWW} distributions especially in high regions. In order to reduce the effects caused by jet radiation subprocesses and keep the convergence of perturbative calculation, we take also the exclusive selection scheme with a jet veto, e.g. in condition of $p_T^{jet} > p_{T,lower}^{jet} = 50$ GeV, then both the overwhelming NLO QCD and photon-induced EW corrections are dramatically suppressed.

Acknowledgments

This work was supported in part by the National Natural Science Foundation of China (No.11275190, No.11375008, No.11375171, No.11405173, No.11535002).

References

- [1] ATLAS collaboration, G. Aad et al., *Observation of a new particle in the search for the Standard Model Higgs boson with the ATLAS detector at the LHC*, Phys. Lett. **B 716** (2012) 1 [arXiv:1207.7214].
- [2] CMS collaboration, S. Chatrchyan et al., *Observation of a new boson at a mass of 125 GeV with the CMS experiment at the LHC*, Phys. Lett. **B 716** (2012) 30 [arXiv:1207.7235].
- [3] S. Godfrey, *Quartic gauge boson couplings*, [hep-ph/9505252].
- [4] O.J.P. Éboli, M.C. Gonzalez-Garcia and S.M. Lietti, *Bosonic quartic couplings at CERN LHC*, Phys. Rev. **D 69** (2004) 095005 [hep-ph/0310141].
- [5] J. Butterworth et al., *Les Houches 2013: Physics at TeV Colliders: Standard Model Working Group Report*, [arXiv:1405.1067].
- [6] V. Hankele and D. Zeppenfeld, *QCD corrections to hadronic WWZ production with leptonic decays*, Phys. Lett. **B 661** (2008) 103 [arXiv:0712.3544].
- [7] A. Lazopoulos, K. Melnikov and F. Petriello, *QCD corrections to triboson production*, Phys. Rev. **D 76** (2007) 014001 [hep-ph/0703273].
- [8] F. Campanario, V. Hankele, C. Oleari, S. Prestel and D. Zeppenfeld, *QCD corrections to charged triple vector boson production with leptonic decay*, Phys. Rev. **D 78** (2008) 094012 [arXiv:0809.0790].
- [9] T. Binoth, G. Ossola, C.G. Papadopoulos and R. Pittau, *NLO QCD corrections to tri-boson production*, JHEP **06** (2008) 082 [arXiv:hep-ph/0804.0350].

- [10] G. Bozzi, F. Campanario, V. Hankele and D. Zeppenfeld, *Next-to-leading order QCD corrections to $W^+W^-\gamma$ and $ZZ\gamma$ production with leptonic decays*, Phys. Rev. **D 81** (2010) 094030 [arXiv:0911.0438].
- [11] G. Bozzi, F. Campanario, M. Rauch and D. Zeppenfeld, *$Z\gamma\gamma$ production with leptonic decays and triple photon production at next-to-leading order QCD*, Phys. Rev. **D 84** (2011) 074028 [arXiv:1107.3149].
- [12] U. Baur, D. Wackerroth and M.M. Weber, *Radiative corrections to $W\gamma\gamma$ production at the LHC*, PoS RADCOR2009 **067** (2010) [arXiv:1001.2688].
- [13] G. Bozzi, F. Campanario, M. Rauch and D. Zeppenfeld, *$W\gamma\gamma$ production with leptonic decays at next-to-leading order QCD*, Phys. Rev. **D 83** (2011) 114035 [arXiv:1103.4613].
- [14] G. Bozzi, F. Campanario, M. Rauch, H. Rzehak and D. Zeppenfeld, *NLO QCD corrections to $W^\pm Z\gamma$ production with leptonic decays*, Phys. Lett. **B 696** (2011) 380 [arXiv:1011.2206].
- [15] D.T. Nhung, L.D. Ninh and M.M. Weber, *NLO corrections to WWZ production at the LHC*, JHEP **12** (2013) 096 [arXiv:1307.7403].
- [16] Shen Yong-Bai, Zhang Ren-You, Ma Wen-Gan, Li Xiao-Zhou, Zhang Yu, Guo Lei, *NLO QCD + NLO EW corrections to WZZ productions with leptonic decays at the LHC*, JHEP **10** (2015) 186 [arXiv:1507.03693].
- [17] U. Baur, T. Han, N. Kauer, R. Sobey and D. Zeppenfeld, *$W\gamma\gamma$ production at the Fermilab Tevatron collider: Gauge invariance and radiation amplitude zero*, Phys. Rev. **D 56** (1997) 140 [hep-ph/9702364].
- [18] P.J. Bell, *Quartic gauge couplings and the radiation zero in $pp \rightarrow \ell^\pm \nu \gamma \gamma$ events at the LHC*, Eur. Phys. J. **C 64** (2009) 25 [arXiv:0907.5299].
- [19] E. Accomando, A. Denner and C. Meier, *Electroweak corrections to $W\gamma$ and $Z\gamma$ production at the LHC*, Eur. Phys. J. **C 47** (2006) 125 [hep-ph/0509234].
- [20] A. Denner, S. Dittmaier, M. Hecht and C. Pasold, *NLO QCD and electroweak corrections to $W + \gamma$ production with leptonic W -boson decays*, JHEP **04** (2015) 018 [arXiv:1412.7421].
- [21] E. Boos et al., *Generic user process interface for event generators*, [hep-ph/0109068].
- [22] J. Alwall et al., *A standard format for Les Houches Event Files*, Comput. Phys. Commun. **176** (2007) 300 [hep-ph/0609017].
- [23] S. Frixione, E. Laenen, P. Motylinski, and B.R. Webber, *Angular correlations of lepton pairs from vector boson and top quark decays in Monte Carlo simulations*, JHEP **04** (2007) 081 [hep-ph/0702198].
- [24] P. Artoisenet, R. Frederix, O. Mattelaer, and R. Rietkerk, *Automatic spin-entangled decays of heavy resonances in Monte Carlo simulations*, JHEP **03** (2013) 015 [arXiv:1212.3460].
- [25] J. Alwall et al., *The automated computation of tree-level and next-to-leading order differential cross sections, and their matching to parton shower simulations*, JHEP **07** (2014) 079 [arXiv:1405.0301].
- [26] A. Denner, *Techniques for the calculation of electroweak radiative corrections at the one-loop level and results for W -physics at LEP200*, Fortschr. Phys. **41** (1993) 307 [arXiv:0709.1075].
- [27] S. Dittmaier and M. Kramer, *Electroweak radiative corrections to W -boson production at hadron colliders*, Phys. Rev. **D 65** (2002) 073007 [hep-ph/0109062].

- [28] T. Hahn, *Generating Feynman diagrams and amplitudes with FeynArts 3*, Comput. Phys. Commun. **140** (2001) 418 [hep-ph/0012260].
- [29] T. Hahn and M. Pérez-Victoria, *Automated one-loop calculations in four and D dimensions*, Comput. Phys. Commun. **118** (1999) 153 [hep-ph/9807565].
- [30] A. Denner, S. Dittmaier, *Reduction of one-loop tensor 5-point integrals*, Nucl. Phys. **B 658** (2003) 175 [hep-ph/0212259].
- [31] G. Passarino and M. Veltman, *One-loop corrections for e^+e^- annihilation into $\mu^+\mu^-$ in the Weinberg model*, Nucl. Phys. **B 160** (1979) 151.
- [32] G.J. van Oldenborgh, *FF - a package to evaluate one-loop Feynman diagrams*, Comput. Phys. Commun. **66** (1991) 1.
- [33] B.W. Harris and J.F. Owens, *Two cutoff phase space slicing method*, Phys. Rev. **D 65** (2002) 094032 [hep-ph/0102128].
- [34] T. Kinoshita, *Mass singularities of Feynman amplitudes*, J. Math. Phys. **3** (1962) 650.
- [35] T. Lee and M. Nauenberg, *Degenerate Systems and Mass Singularities*, Phys. Rev. **133** (1964) B1549.
- [36] ATLAS collaboration, G. Aad et al., *Measurement of the transverse momentum distribution of Z/γ^* bosons in proton-proton collisions at $\sqrt{s} = 7$ TeV with the ATLAS detector*, Phys. Lett. **B 705** (2011) 415 [arXiv:1107.2381].
- [37] PARTICLE DATA GROUP collaboration, K.A. Olive et al., *Review of particle physics*, Chin. Phys. **C 38** (2014) 090001.
- [38] NNPDF collaboration, R.D. Ball et al., *Parton distributions with QED corrections*, Nucl. Phys. **B 877** (2013) 290 [arXiv:1308.0598].
- [39] K.-P. O. Diener, S. Dittmaier, and W. Hollik, *Electroweak higher-order effects and theoretical uncertainties in deep-inelastic neutrino scattering*, Phys. Rev. **D 72** (2005) 093002 [hep-ph/0509084].
- [40] A. Denner and S. Pozzorini, *One-loop leading logarithms in electroweak radiative corrections I. Results*, Eur. Phys. J. **C 18** (2001) 461 [hep-ph/0010201].
- [41] A. Denner and S. Pozzorini, *One-loop leading logarithms in electroweak radiative corrections II. Factorization of collinear singularities*, Eur. Phys. J. **C 21** (2001) 63 [hep-ph/0104127].